ACS APPLIED MATERIALS & INTERFACES

Research Article

www.acsami.org

Layer-by-Layer Assembly of Graphene Oxide Nanosheets on Polyamide Membranes for Durable Reverse-Osmosis Applications

Wansuk Choi,[†,‡] Jungkyu Choi,*[,†,⊥] Joona Bang,*[,†] and Jung-Hyun Lee*[,‡]

[†]Department of Chemical and Biological Engineering, Korea University, 5-1 Anam-dong, Seongbuk-gu, Seoul 136-713, Republic of Korea

[‡]Center for Materials Architecturing, Korea Institute of Science and Technology, 39-1 Hawolgok-dong, Seongbuk-gu, Seoul 136-791, Republic of Korea

[⊥]Green School, Korea University, 5-1 Anam-dong, Seongbuk-gu, Seoul 136-713, Republic of Korea

Supporting Information

ABSTRACT: Improving membrane durability associated with fouling and chlorine resistance remains one of the major challenges in desalination membrane technology. Here, we demonstrate that attractive features of graphene oxide (GO) nanosheets such as high hydrophilicity, chemical robustness, and ultrafast water permeation can be harnessed for a dual-action barrier coating layer that enhances resistance to both fouling and chlorine-induced degradation of polyamide (PA) thin-film composite (TFC) membranes while preserving their separation performance. GO multilayers were coated on the PA-TFC membrane surfaces via layer-by-layer (LbL) deposition of oppositely charged GO nanosheets. Consequently, it was shown that the conformal GO coating layer can increase the surface hydrophilicity and reduce the surface roughness, leading to the significantly improved antifouling performance against a protein foulant. It was also demonstrated that the chemically inert nature of GO nanosheets enables the GO coating layer to act as a chlorine barrier for the underlying PA membrane, resulting in a profound suppression of the membrane degradation in salt rejection upon chlorine exposure.

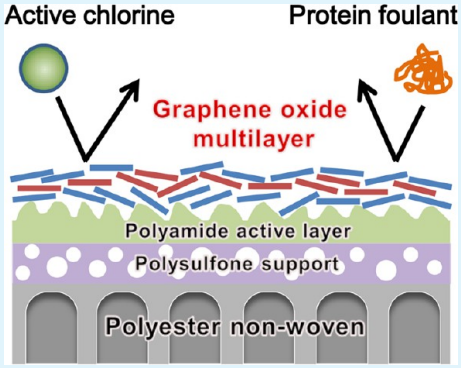

KEYWORDS: *reverse osmosis membrane, graphene oxide, layer-by-layer assembly, fouling resistance, chlorine resistance*

INTRODUCTION

The membrane desalination process of reverse osmosis (RO) has become a leading technology for the sustainable production of freshwater from saline sources.[1−4] Most of the currently available commercial RO membranes adopt a thin-film composite (TFC) configuration, as exemplified by an interfacially polymerized, fully aromatic polyamide (PA) selective layer on top of a microporous support membrane, where the PA layer plays a dominant role in the membrane permselectivity.[3] Although these PA-based membranes are capable of discriminating a wide range of solutes, they often suffer from performance deterioration, because of membrane fouling. This fouling, which ultimately shortens the operating lifetime of RO membranes, can be considered as a process by which various matter such as proteins, micro-organisms, and inorganic colloids settle and accumulate on the membrane surface and disfavor the permeation of desired molecules.[3,5,6] To prevent and inhibit the degree of fouling, chlorine or chlorine-based chemicals have been commonly used as disinfecting agents in membrane systems, although the fully aromatic PA membrane is highly susceptible to concomitant oxidative degradation by chlorine, and, thus, the use of chlorine is not desired for reliable application of PA-based membranes.[3] Despite the progress made over the last few decades, there is still considerable need for improvements in PA-based membrane durability associated with antifouling and chlorine resistance.

To date, several methods have been explored to cope with the aforementioned two major drawbacks, including the membrane surface modification via the coating or grafting of functional materials,[7−10] the incorporation of nanomaterials into membranes,[11,12] and the fabrication of new membranes with tailored chemistry.[13−15] Among them, the membrane surface coating is generally regarded as the most efficient approach, because of its facile processability. Although an additional surface coating can improve membrane durability, the undesired reduction in water flux is usually observed, following the typical trade-off relation between performance and durability.[3] In addition, it has been recognized that the coating strategy to enhance both antifouling capability and chlorine resistance is highly desirable to achieve the practical long-term durability of the membrane.[16] For example, antifouling membranes are still required to have a certain level of chlorine resistance, since they are hardly exposed to the

Received: September 4, 2013
Accepted: November 12, 2013
Published: November 12, 2013

free chlorine environment during the actual operating process. Similarly, chlorine-resistant membranes do not necessarily offer a complete solution for membrane fouling, because chlorine cannot deactivate all nonbiological matter and/or biological organisms that have the self-replicating nature to regenerate biofouling. However, most studies have relied exclusively either on reducing fouling propensity or on improving chlorine resistance,[5,17] but rarely on combining both strategies for synergic effects. Hence, there is a growing demand for the unified coating strategy that enhances resistance to both fouling and chlorine-induced degradation, while retaining the flux and salt rejection performance of the original membrane.

Graphene oxide (GO) is a single sheet of graphene functionalized with oxygen-rich functional groups in the form of carboxyl, hydroxyl, ether, and epoxy groups.[18] Recently, GO nanosheets have attracted special interest in the field of water purification membrane, because of their unique transport properties.[19−21] Many efforts have been made to fabricate highly permeable membranes by taking advantage of the extremely fast water transport along the nanochannels between graphene nanosheets. For example, in a recent work, reduced GO sheets were deposited by filtration on porous substrates,[22] allowing the preferred water permeation with a modest NaCl rejection rate (∼40%). Also, the layer-by-layer (LbL) approach via the bonding between GO sheets and trimesoyl chloride (TMC) succeeded in securing the NaCl rejection performance (∼20%−30%), which otherwise could not be realized simply by using the polysulfone support.[20] In addition, an approach to attain the synergic effect of carbon nanotube and reduced GO composites was proposed and shown to be promising for the water desalination.[23] Along with the desalination purpose, homogenous GO membranes were physically fabricated on porous substrates and exhibited a high molecular sieving ability for H_2 and/or CO_2 gas separations.[24,25] However, little attention has been paid to other useful properties of GO that can be used to improve membrane durability. For example, coating membrane surfaces with highly hydrophilic, planar GO nanosheets can suppress the fouling by hydrophobic foulants.[18] Furthermore, GO's excellent chemical stability could potentially be utilized as a protective coating layer for PA membranes against chlorine attack.[26] Together with the highly water permeable nature of GO sheets, the GO surface coating can be an excellent candidate to improve both antifouling and chlorine resistance of membranes at the same time.[19−21,27]

In this study, we demonstrate that the coating of GO nanosheets on the surface of the fully aromatic PA-TFC membrane serves as a dual-functional protective layer to improve both membrane antifouling and chlorine resistance, while maintaining its separation performance. Specifically, we employed the LbL technique to deposit GO multilayers on the membrane surface, because it is a simple, but reliable method to create conformal GO assembly in a controllable manner. A pair of oppositely charged GO nanosheets (positively charged, aminated-GO (AGO) and negatively charged GO) were alternatingly deposited on the interfacially polymerized PA membrane surface primarily through electrostatic interaction. We first investigated the effect of the GO coating on the membrane performance (water flux and NaCl salt rejection) and it was found that the membrane performance was essentially unchanged by the GO coating. Then, we monitored the flux change of the membrane during the filtration with the feed solution containing a model protein foulant (bovine serum albumin, BSA) to assess membrane antifouling performances. Also, the chlorine stability of the same GO multilayer-coated PA membrane was examined by comparing the membrane performance before and after chlorination. Consequently, the GO assembly on the membrane surface significantly mitigated membrane fouling against hydrophobic BSA molecules (an ultimate flux decline of ∼15% vs ∼34% for the pristine PA membrane after 12 h of exposure) and, at the same time, improved membrane chlorine resistance by effectively retarding the selectivity deterioration upon chlorine exposure (a rejection reduction of ∼4% vs ∼50% for the pristine PA membrane after 1 h of treatment of 6000 mg/L NaOCl). It appears that such a stability improvement can be attributed to the role of GO nanosheets as protective layers that disfavor the adsorption of hydrophobic proteins on the PA surface due to their hydrophilicity and retard diffusion of active chlorine species (OCl^- ions) toward the middle core area of the PA selective layers, because of their transport resistance.

EXPERIMENTAL SECTION

Materials. The following chemicals were used as received: graphite powder (synthetic, <20 μm in size, Sigma−Aldrich), nitric acid (HNO_3; fuming, 90%, Junsei Chemical), potassium chlorate ($KClO_3$; Sigma−Aldrich), ethylenediamine (Sigma−Aldrich), 1-(3-dimethylaminopropyl)-3-ethylcarbodiimide methiodide (EDC; Sigma−Aldrich), *m*-phenylenediamine (MPD; Sigma−Aldrich), trimesoyl chloride (TMC; Sigma−Aldrich), triethylamine (TEA; > 99.5% Sigma−Aldrich), sulfuric acid (H_2SO_4; 95%, Sigma−Aldrich), sodium chloride (NaCl; Sigma−Aldrich), sodium hydroxide (NaOH; Fluka), sodium hypochlorite (NaOCl; 4% aqueous solution, Sigma−Aldrich), ethanol (> 95%, J.T. Baker), *n*-hexane (> 95%, J.T. Baker), and bovine serum albumin (BSA; Sigma−Aldrich). Deionized (DI) water (18.2 MΩ cm) was prepared in a Millipore Milli-Q purification system. Polysulfone (PSf) ultrafiltration membrane (UE50) with a polyester nonwoven as a support was obtained from Trisep Co.

Preparation of GO and Aminated-GO (AGO) Nanosheets. GO nanosheets were prepared from graphite powder by the modified Brodie method.[28] In brief, 2 g of graphite powder was added to 75 g of the solution with mass ratio of 3.1 HNO_3/1.0 $KClO_3$, and then oxidized by stirring the mixture at room temperature for 12 h. The resulting mixture was diluted with DI water, and subsequently centrifuged at least three times to obtain purified GO nanosheets. AGO nanosheets were prepared through further modification of the prepared GO nanosheets by using the method described in the literature.[29−31] Briefly, 2 g of GO nanosheets was dispersed in 100 mL of ethanol by sonication for 2 h, followed by the addition of 5 g of ethylenediamine and 0.5 g of EDC, the latter being added as a coupling agent that can induce the amide formation between the carboxylic acid group of GO and the amine terminal group of ethylenediamine. The resulting solution was stirred at room temperature for 12 h, and then washed with DI water via at least three centrifugation cycles.

Preparation of PA-TFC Membrane. A crosslinked, fully-aromatic PA selective layer was synthesized on a microporous PSf/polyester non-woven support via interfacial polymerization of MPD and TMC monomers to prepare a PA-TFC membrane. The PSf support was first rinsed with DI water and then immersed into a MPD (1.0 wt %) solution in water for 3 min. TEA (0.1 wt %) was also added as an acid acceptor in the MPD solution. Excess MPD solution was removed by rolling with a rubber roller. Subsequently, the membrane was soaked into a TMC (0.1 wt %) solution in *n*-hexane for 1 min and rinsed with clean *n*-hexane, followed by drying at 70 °C for 10 min.

Surface Modification of PA-TFC Membrane with GO Multilayer. The surface of the prepared PA-TFC membrane was modified by depositing a GO multilayer onto the PA selective layer (referred to here as "GO-coated PA membrane") via LbL deposition of oppositely charged GO and AGO nanosheets. Aqueous suspensions of negatively charged GO (1.0 wt %) and positively charged AGO (1.0 wt %) were prepared by sonication for 1 h to ensure a uniform

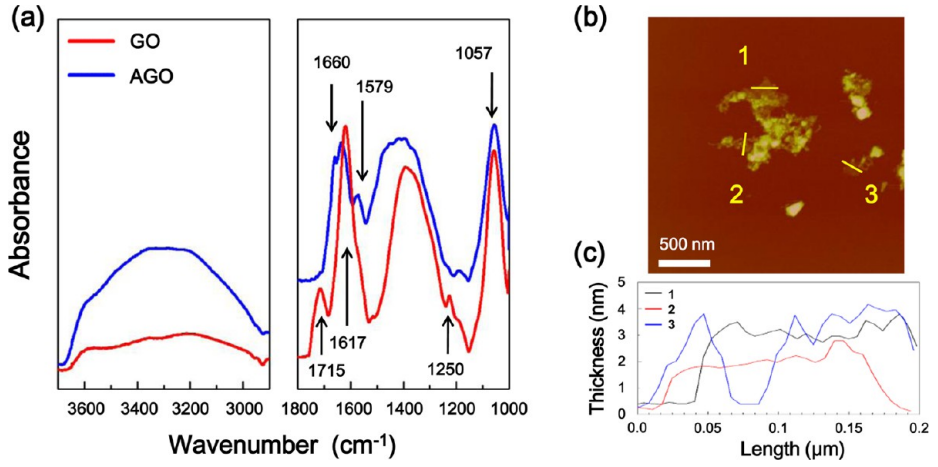

Figure 1. (a) FT-IR spectra of graphene oxide (GO) and aminated-GO (AGO) nanosheets. (b) AFM topographic image of GO nanosheets. (c) Cross-sectional height profiles along the lines marked in panel b.

dispersion of nanosheets. The pH values of the GO and AGO aqueous suspensions were adjusted to 3.0 and 10.0, respectively. The PA membrane, whose surface is known to have a negative charge, was first dipped into the aqueous suspension of positively charged AGO for 10 min, followed by rinsing with DI water. Then, the membrane was immersed into the aqueous suspension of negatively charged GO for 10 min and subsequently rinsed with DI water. This process completes one cycle of LbL deposition to form one bilayer of AGO/GO. The deposition cycle was repeated until the desired number of AGO/GO bilayers ("AGO/GO bilayer" is simply referred to as "GO bilayer") was obtained. After LbL deposition was finished, the membrane was dried at 70 °C for 10 min. For comparison, the "GO-underlaid PA membrane" and "GO-sandwiched PA membrane" were also prepared: in the former, the GO multilayer was placed between the PSf support and the PA layer; in the latter, it was coated on both sides of the PA layer. For the preparation of the GO-underlaid PA membrane, the PSf support was first treated with an aqueous solution of H_2SO_4 (5.0 wt %) at 80 °C for 30 min to impart the negative charge on the PSf surface.[32] Next, the GO multilayer was deposited on the surface of the acid-treated PSf support by following the above-mentioned LbL protocol. Subsequently, the PA selective layer was fabricated on the GO-coated PSf membrane via interfacial polymerization process as described above. To prepare the GO-sandwiched PA membrane, the surface of the fabricated GO-underlaid PA membrane (i.e., the top side of the PA layer) was further coated by LbL deposition of GO multilayer.

Characterization of GO Nanosheets and Membranes. The chemical structures of the GO and AGO nanosheets and membranes were characterized by Fourier transform infrared (FT-IR) and X-ray photoelectron spectroscopy (XPS) analyses. FT-IR was performed on a Nicolet IS10 spectrometer (ThermoFischer Scientific) equipped with an attenuated total reflectance unit. XPS spectra were recorded on a PHI-5000 Versaprobe spectrometer using monochromatized Al Kα radiation at 1486.6 eV. The surface zeta potentials of the GO and AGO nanosheets and membranes were determined with an electrophoretic measurement apparatus (ELSZ, Otsuka Electronics). The zeta potential was measured in a background aqueous solution of NaCl (10 mM) containing mobility-monitoring particles. A plate sample cell was used for all membrane samples. The morphology and thickness of the GO nanosheets were characterized using an atomic force microscopy (AFM) (Veeco Nanoscope V) operated in tapping mode. The surface morphologies of the membranes were examined by scanning electron microscopy (SEM) (FEI Inspect F50) and atomic force microscopy (AFM). SEM micrographs of membrane surfaces were obtained at an accelerating voltage of 10 kV. The arithmetic average (R_a) roughness of membranes was estimated from the topography images of 5 μm × 5 μm area. Water contact angles of the membrane surfaces were measured with a goniometer (NRL CA Goniometer, Rame-Hart, Inc.) equipped with a video capture apparatus at room temperature. The averaged contact angle was determined from eight measurements for each sample.

Membrane Performance Tests. Membrane performance was assessed with 2000 mg/L NaCl aqueous solution at pH 5.8 in a cross-flow system with an effective area (A) of 13.85 cm^2. Water flux and salt rejection were determined under an operating pressure of 15.5 bar at room temperature. Permeate flux was automatically recorded by a digital balance and performance data were measured after steady flux had been reached. Water flux (F) was determined from the total amount of the collected permeate (V) for a fixed time (t), as described by F (L/(m^2 h)) = V/At. Salt concentrations of permeate (C_p) and feed (C_f) were measured with a conductivity meter (Eutech PC650), and salt rejection (R) was calculated by the following equation: R (%) = 100 × (1 − C_p/C_f).

Membrane Fouling Tests. Membrane fouling was evaluated from filtration experiments with an aqueous feed solution containing a model protein foulant (BSA) using the cross-flow apparatus. The membrane was first stabilized with DI water at an operating pressure of 15.5 bar for 12 h. After water flux reached a steady state, a certain amount of BSA was instantaneously added to the feed reservoir to make the concentration of 100 mg/L, and permeate flux was recorded at the time interval of 1 h. The extent of membrane fouling was assessed by the relative water flux, which is the measured flux normalized by the initial value.

Membrane Chlorine Stability Tests. The chlorine solution was prepared by diluting a commercial sodium hypochlorite stock solution (4% NaOCl aqueous solution) in DI water to make the chlorine concentration of 6000 mg/L. Since alkaline solutions are often used as cleaning agents,[33] we prepare the chlorine solution at high pH (pH 10), which was achieved by a simple dilution without additional pH adjustment. Chlorination was performed by soaking membrane samples in the prepared chlorine solution (chlorine concentration = 6000 mg/L, pH 10) for different periods of exposure time (t_{exp}, 0−12 h). After chlorination, samples were rinsed thoroughly with DI water prior to measurement. Water flux and salt rejection of the pristine PA and the GO-coated PA membranes were measured before and after chlorination, and the chlorine stability for each membrane was evaluated from the extent of performance change after chlorine exposure.

RESULTS AND DISCUSSION

Properties of GO and AGO Nanosheets. Figure 1a shows FT-IR spectra of the GO and AGO nanosheets. GO exhibited the characteristic peaks at 1057 cm^{-1} (C−O stretching), 1250 cm^{-1} (C−OH stretching), 1617 cm^{-1} (C═C bonds), and 1715 cm^{-1} (carboxylic acid C═O stretching),

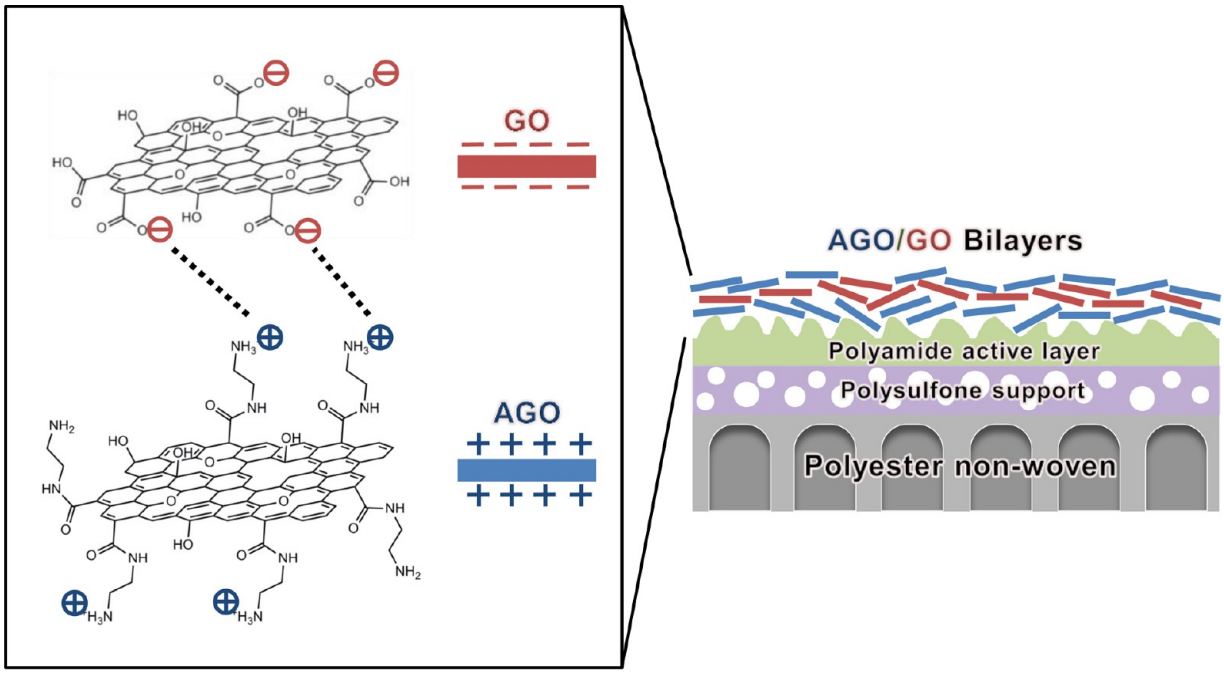

Figure 2. Schematic illustration of a multilayered graphene oxide (GO) coating on a polyamide thin-film composite membrane surface via layer-by-layer (LbL) deposition of oppositely charged GO and aminated-GO (AGO) nanosheets.

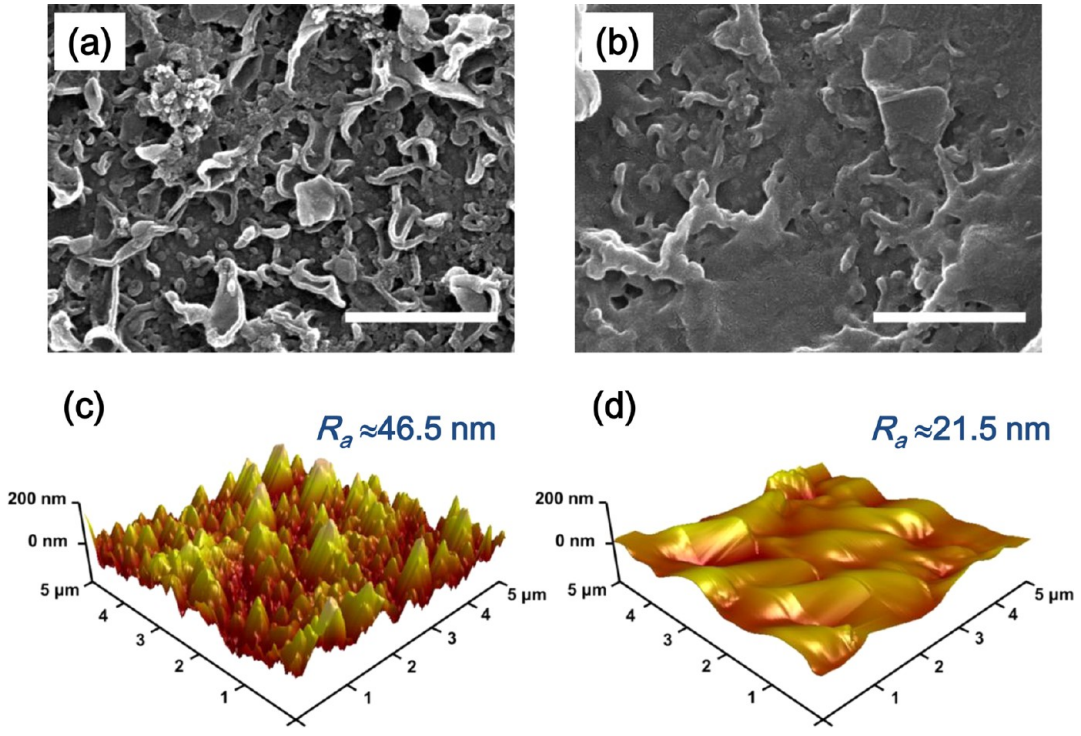

Figure 3. Top-down SEM images of (a) the pristine, uncoated polyamide (PA) and (b) the GO_{10}-coated PA membranes (scale bar = 1 μm). AFM height images of (c) the pristine PA and (d) the GO_{10}-coated PA membranes.

together with a broad band at ~3300 cm^{-1} (O−H stretching).[34−37] The observed FT-IR spectra indicate that GO nanosheets contain ether, epoxy, carboxylic acid, and hydroxyl functional groups. For the AGO, the peak according to the carbonyl group appeared at 1660 cm^{-1} (amide C═O stretching) instead of at 1715 cm^{-1} (carboxylic acid C═O stretching),[31] verifying the formation of amide linkages between the carboxylic acid on GO and the terminal amine of ethylenediamine. In addition, the appearance of a new peak at 1579 cm^{-1} (N−H in-plane stretching) and the intensification of the broad band at ~3300 cm^{-1} (N−H stretching) indicate the deposition of amine functional groups on GO and further support the successful modification of GO with amine functional groups to prepare AGO.[31,38] Zeta potential measurements revealed that the GO and AGO nanosheets had a surface charge of −25.7 ± 0.7 mV at pH 3.0 and +20.6 ± 1.1 mV at pH

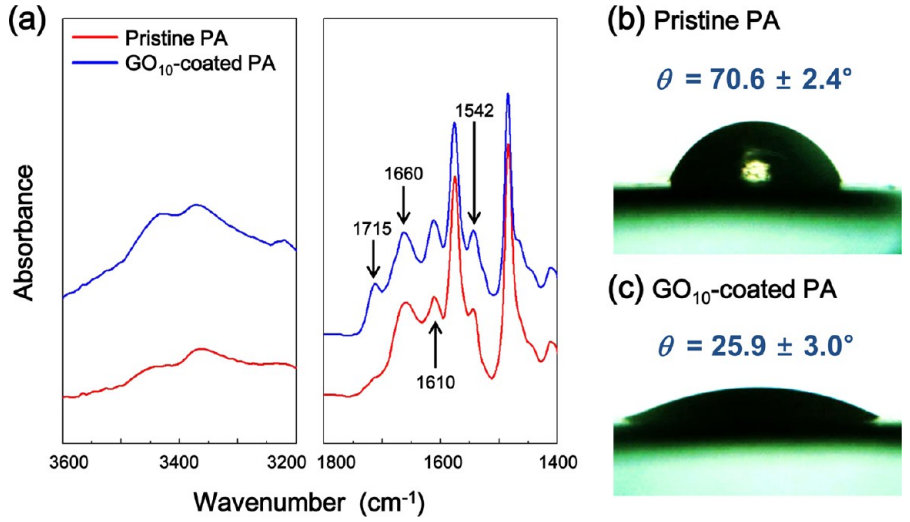

Figure 4. (a) FT-IR spectra of the pristine, uncoated polyamide (PA) and the GO_{10}-coated PA membranes. The representative images of water contact angles on (b) the pristine PA and (c) the GO_{10}-coated PA membranes.

10.0, respectively. This result, together with FT-IR results, shows that the GO nanosheets are negatively charged at pH 3.0, mainly due to the presence of carboxylic acid groups, while the AGO nanosheets are positively charged at pH 10.0, because of amine functional groups. The morphology of individual GO nanosheets was examined by atomic force microscopy (AFM). The sample was prepared by dipping a silicon surface into a diluted GO suspension for several seconds and then dried under air. As seen in Figures 1b and 1c, the lateral dimension of the GO nanosheets ranges from 20 nm to 2000 nm, and GO thickness was estimated to be 2−4 nm, indicating that the prepared GO nanosheets consist of 2−4 graphene layers.

Membrane Modification and Properties. Figure 2 depicts the LbL deposition of AGO and GO nanosheets on the PA-TFC membrane surface. For convenience, a PA-TFC membrane is shortened to a PA membrane. The PA membrane was first dipped into an aqueous suspension of positively charged aminated-GO (AGO), and the deposition of AGO layer is favored by the negative charge of carboxylic acid groups on the PA surface resulting from the hydrolysis of unreacted TMC.[39] Then, negatively charged GO was deposited through electrostatic interaction to create a pair of AGO/GO layers (referenced as one GO bilayer). The sequential AGO/GO depositions were repeated until the desired number of GO bilayers was reached. The LbL-assembled GO multilayers are denoted as GO_x, where x is the number of bilayers. Besides dominant electrostatic forces, hydrogen bonding between uncharged functional groups (e.g., amine, carboxylic acid, and hydroxyl groups) on the AGO and GO sheets is likely to reinforce the stability of the GO multilayer.[26] To verify the stability of the GO-coated PA membrane, presumably endowed with electrostatic force and also hydrogen bonding, we performed the long-term filtration test in a cross-flow system for 72 h and verified good resistance of the GO layer against detachment and delamination from the PA surface by characterizing the surface morphology and water contact angle of the membrane after the filtration test (see Figure S1 in the Supporting Information). Furthermore, we confirmed the stability of the GO multilayer, when the GO-coated membrane is exposed to the various operating pHs (4−10) (Figure S2 in the Supporting Information) and to the pressurized chlorine solution (Figure S3 in the Supporting Information).

The surface morphology of the GO_{10}-coated PA membrane was compared with the pristine, uncoated PA membrane (Figure 3). The pristine PA membrane surface exhibited a rough ridge-and-valley structure, which is a typical characteristic of interfacially polymerized, fully-aromatic PAs (see Figure 3a).[1] After LbL deposition of planar AGO and GO nanosheets on the PA membrane, it can be clearly seen that the membrane surface is significantly smoothened by filling the valley regions of the rough PA surface with GO sheets (Figure 3b). AFM estimated the arithmetic average (R_a) roughness of the GO_{10}-coated PA membrane to be ~21.5 nm, much lower than that of the pristine PA membrane (~46.5 nm) (see Figures 3c and 3d). It was also found that the high level of GO coverage was achieved by 10 GO bilayers, although the membrane surface was not completely covered by GO sheets.

FT-IR and X-ray photoelectron spectroscopy (XPS) were performed to characterize the chemical structures of the pristine PA and GO_{10}-coated PA membranes. As shown in Figure 4a, the pristine PA membrane had characteristic peaks at 1660 cm^{-1} (amide I, C═O stretching), 1610 cm^{-1} (hydrogen-bonded C═O), and 1542 cm^{-1} (amide II, N−H in-plane bending) and a broad band at ~3400 cm^{-1} (N−H stretching).[38] For the GO_{10}-coated PA membrane, the peak at 1715 cm^{-1} (carboxylic acid C═O stretching) was pronounced and the broad band at ~3400 cm^{-1} was intensified, compared to that of the pristine one. These spectral differences could be attributed to the carboxylic acid, hydroxyl, and amine groups rich in GO nanosheets that constituted the GO_{10}-coated PA membrane.[18,40] From XPS results, the oxygen atomic content of the GO_{10}-coated PA membrane was determined to be 15.3 ± 1.3, apparently higher than that of the pristine PA membrane (13.4 ± 0.4), indicating the presence of oxygen-containing carboxylic acid and hydroxyl groups. Such observation was in good agreement with the FT-IR results that also demonstrated the abundance of the oxygen-containing carboxylic acid and hydroxyl groups in the GO_{10}-coated PA membrane.

Wettability, evaluated by the water contact angle, is an important surface property that can be correlated strongly with the membrane performance as well as fouling. The GO_{10}-

coated PA membrane exhibited a remarkably lower contact angle ($\theta = 25.9° \pm 3.0°$) than that of the pristine PA membrane ($\theta = 70.6° \pm 2.4°$) (Figures 4b and 4c), illustrating that the GO coating enhances the membrane wettability likely associated with the hydrophilic nature of constituent GO sheets. Both AGO and GO nanosheets are readily dispersed in aqueous media, because of their strong hydrophilicity originating from a high density of hydrophilic functional groups present on their surfaces, thereby leading to the hydrophilic surface coating on the PA membranes.[18]

Membrane Performance. To evaluate the effect of the GO surface coating on the membrane performance, the water flux and salt (NaCl) rejection of the GO-coated PA membranes were measured as a function of the number of GO bilayers (Figure 5). The pristine PA membrane (equivalent to 0 bilayer)

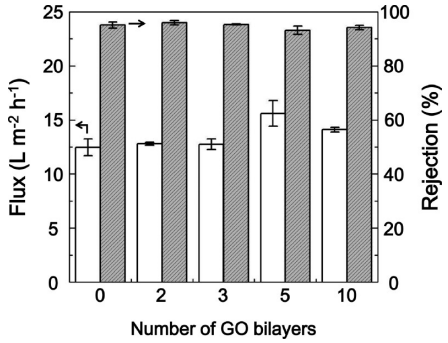

Figure 5. Water flux and NaCl rejection of the GO-coated polyamide (PA) membranes as a function of the number of GO bilayers. Note that 0 bilayer corresponds to the pristine, uncoated PA membrane. All performance measurements were conducted using an aqueous solution of NaCl (2000 mg/L) at an operating pressure of 15.5 bar.

exhibited water flux of (12.5 ± 0.8) L/(m^2 h) and salt rejection of 97.1% ± 1.1%. Interestingly, it was found that the membrane performance after GO surface coating remained essentially unchanged within measurement errors, regardless of the number of GO bilayers. For example, the water flux and salt rejection of the GO_{10}-coated PA membrane were estimated to be 14.0 ± 0.3 L/(m^2 h) and 96.4% ± 0.9%, respectively, comparable to those of the pristine PA membrane. This result is quite intriguing, since one would expect that the GO surface coating will reduce the water flux by increasing the hydrodynamic resistance and also by reducing the effective contact area resulting from the smoothened surface.[41] In fact, this result is in qualitative agreement with the previous experimental observation that water permeability of the LbL-assembled, multilayered GO membrane was not a strong function of the multilayer thickness. This phenomena was attributed presumably to the unique water transport (a nearly frictionless, ultrafast water flow) through the stacked GO nanosheets.[20] In this vein, the observation in our system suggests that increasing the surface hydrophilicity via the GO coating, as well as the extremely high water permeability of the GO nanochannels, possibly overwhelm the flux loss by hydrodynamic resistance.

Membrane Fouling. We first utilized GO's beneficial properties, strong hydrophilicity and planar geometry, to improve antifouling performance. It is known that the morphological and physicochemical properties of membrane surfaces strongly affect the fouling behavior.[41,42] More hydrophilic and smoother surface of the GO-coated PA membrane is expected to bear better antifouling capability than the uncoated PA membrane.[41,42] To verify this, we monitored the relative water flux of the GO_{10}-coated PA membrane as a function of operation time during the filtration with aqueous solution of BSA (100 mg/L), in comparison with the pristine PA membrane (Figure 6). In the case of the pristine

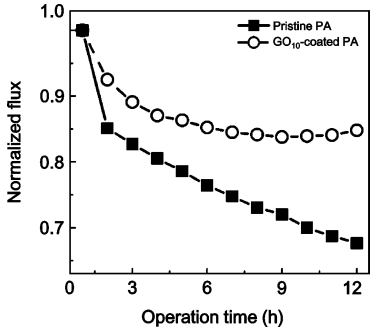

Figure 6. Normalized water flux of the pristine, uncoated polyamide (PA) and the GO_{10}-coated PA membranes as a function of filtration time upon the addition of BSA foulants (100 mg/L). The normalized flux was obtained by dividing the measured value after a certain operation time by the initial flux value.

PA membrane, water flux decreased rapidly in the early period of the filtration, and then decreased monotonically (almost linearly) with increasing filtration time up to 12 h. In contrast, for the GO_{10}-coated PA membrane, water permeation decreased gradually and then reached a plateau at ~6 h. It was noted that the GO_{10}-coated PA membrane exhibited a lower degree of final flux reduction (~15%) after filtration for 12 h than that of the pristine PA membrane (~34%), demonstrating improved antifouling performance by the multilayered GO coating.

The membrane surface charge has been considered to be one of the important properties that determine fouling behavior, in particular related to charged foulants such as BSA which possesses negative charge at pH >4.8.[7] The zeta potential of the GO_{10}-coated PA membrane was measured to be −14.2 ± 2.6 mV under the operating pH condition (pH 5.8), comparable to that of the pristine PA membrane (−30.6 ± 0.2 mV). This indicates that the surface charge and associated electrostatic interaction are not critical to determine the observed fouling behavior in this study; otherwise, fouling would be more pronounced for the GO_{10}-coated PA membrane.[43] Instead, the suppressed fouling in the GO_{10}-coated membrane can be attributed to enhanced hydrophilicity and/or reduced surface roughness imparted by the multilayered GO coating that could minimize the preferential attraction between the hydrophobic BSA molecule and the membrane surface and the possibility of the BSA molecule being stuck in the rough surface, respectively.[7]

Membrane Chlorine Resistance. We further studied the effect of the multilayered GO coating on the chlorine-induced degradation of the membrane. The degradation mechanism of the fully aromatic PA membrane by chlorine has been extensively studied.[3,17,44,45] The membrane failure is usually ascribed to the structural change of the PA selective layer in response to chlorine exposure. The possible chemical mechanism of PA degradation involves chlorine attack on the amide nitrogen (N-chlorination) and aromatic ring (ring chlorination) along with the subsequent amide bond cleavage via hydrolysis, which could disrupt the intermolecular hydrogen

bonds and eventually destroy the PA network.[17,44] This structural change causes conformational deformation associated with enhanced chain flexibility and reduced crosslinking density, typically leading to increased water flux and decreased salt rejection.[3,45]

To evaluate the chlorine stability of the GO-coated membranes prepared in this study, we measured their separation performance before and after chlorine exposure. Performance data of the GO-coated PA membranes after chlorination (for 1 h) normalized by those of their counterparts having the same number of GO bilayers before chlorination were presented as a function of the number of GO bilayers in Figure 7. It was seen that chlorine exposure increased water flux

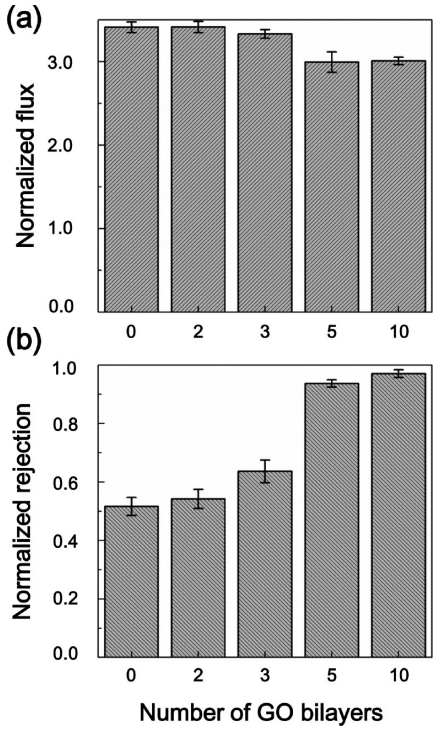

Figure 7. (a) Normalized water flux and (b) normalized NaCl rejection of the chlorinated, GO-coated polyamide (PA) membranes, as a function of the number of GO bilayers (chlorination conditions: chlorine concentration = 6000 mg/L, pH 10, and chlorine exposure time = 1 h). The normalized values were obtained by dividing the measured values of the GO-coated membranes after chlorination by those of their counterparts having the same number of GO bilayers before chlorination.

(e.g., normalized flux of ~3.0 to ~3.3) and reduced salt rejection (i.e., normalized rejection of ~0.5 to ~1.0) for all tested membranes. The extent of increase in water flux by chlorination was generally lower when the PA membranes were coated with a higher number of GO bilayers (see Figure 7a), although the difference was not significant. A more-pronounced effect of the GO coating was observed for the rejection behavior in response to chlorine. While the salt rejection of the uncoated PA membrane (0 bilayer) was dramatically decreased to ~50% upon 1 h of chlorine exposure, the degree of reduction in salt rejection decreased progressively as the number of GO bilayers increased and even reached <4% for the GO_{10}-coated PA membrane, indicating that the remarkable enhancement in resistance to the chlorine-induced degradation of salt rejection was achieved by the GO multilayered coating.

For elucidating the degradation behavior, we further monitored the performance changes of the GO_{10}-coated PA membrane (chosen because of its best performance in this study, as shown in Figure 7) as a function of chlorine exposure time (t_{exp}), in comparison with the pristine PA membrane (Figure 8). As the chlorination time increased, the normalized

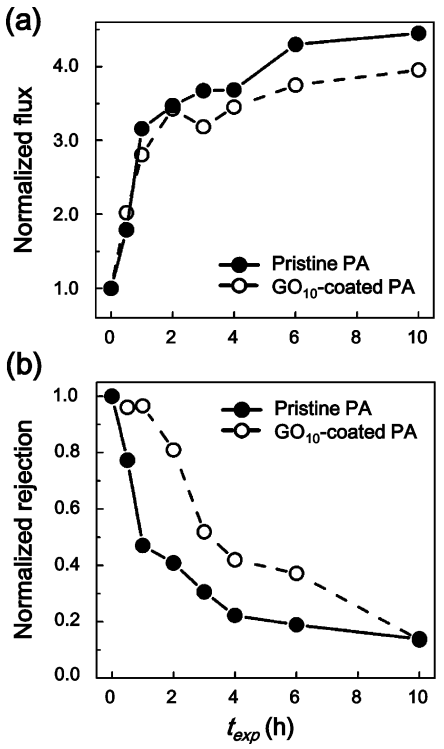

Figure 8. Changes in (a) normalized water flux and (b) normalized NaCl rejection of the pristine, uncoated polyamide (PA) and the GO_{10}-coated PA membranes as a function of chlorine exposure time (t_{exp}; chlorination conditions: chlorine concentration = 6000 mg/L and pH 10). The normalized values were obtained by dividing the measured values of the membranes after chlorination for a certain time by those before chlorination.

water flux increased rapidly before it reached a plateau for both membranes, and no significant difference in the flux levels was observed between them throughout the measured chlorine exposure time (up to 10 h; see Figure 8a). On the other hand, the extent of reduction in salt rejection was effectively suppressed for the GO_{10}-coated membrane, compared to the pristine PA membrane, although increasing the chlorination time continuously deteriorated salt rejection for both membranes (Figure 8b). In particular, in the early stage of chlorination (<1 h), the salt rejection of the GO_{10}-coated membrane remained almost unchanged, while that of the pristine PA membrane was rapidly reduced, suggesting that the multilayered GO coating present on the PA membrane plays an important role in preventing the selectivity deterioration. However, the retarding effect of the GO coating on the rejection loss diminished gradually with increasing chlorination time, and ultimately vanished at the highest chlorine dose (chlorination for 10 h). At this point, we would like to emphasize that, although 10 h of chlorine exposure makes no difference in both GO_{10}-coated and pristine PA membranes, a simulated condition of 6000 mg/L NaOCl solution was quite harsh, compared to those used in some previous studies (e.g.,

10−100 ppm and ∼50 pm).[13,38] Simply considering the exposure level (equivalent to the product of the NaOCl concentration and exposure time (ppm h)), the GO_{10}-coated PA membrane that maintained salt rejection higher than 92.3% ± 2.7% up to 1 h of chlorine exposure under the current NaOCl solution is expected to maintain such salt rejection performance up to ∼8 months of chlorine exposure in ∼1 ppm NaOCl solution at atmospheric pressure.[13]

At first glance, one might argue that the GO multilayer itself could serve as a salt discriminating layer that compensates for the loss of salt rejection of the underlying PA selective layer upon chlorination. However, this is not likely to be the case, since the NaCl rejection of the GO_{10} multilayer solely deposited on a polysulfone (PSf) support (GO_{10} membrane) was estimated to be 12.2% ± 0.6%, implying that the GO multilayer itself does not provide a highly selective separation function for NaCl salt, which is in reasonable agreement with the previous report on the separation performance of the LbL-based GO membranes.[20]

In order to rationalize the observed performance behavior upon chlorine exposure, we looked more closely at the structure of the PA selective layer, because its structural change in response to chlorine determines the membrane permselectivity. The PA layer structure (e.g., molecular density and crosslinking degree) has been reported to be highly depth-heterogeneous, characterized as a densely cross-linked "inner core layer" sandwiched by looser outer layers. Essentially, the inner core layer is mainly responsible for salt rejection, while the bulk density of the PA selective layer determines water permeation.[41,46−49] With this scenario, upon chlorination, reactive chlorine species (OCl^- ion) first attack the outmost layer and then gradually penetrate toward the inner core layer in a way that the enhanced chain flexibility in chlorinated region facilitates the chlorine diffusion. Thus, the salt rejection would not deteriorate unless the inner core layer begins to degrade by prolonged chlorination, although the water flux would be changed continuously with increasing chlorine exposure, because of its dependence on the volume-averaged density of the PA selective layer.

For the chlorination of the GO-coated PA membrane, the chemically robust GO layer is likely to act as a barrier layer that can protect the underlying PA from chlorine attack, as manifested in the highly suppressed reduction rate of salt rejection for the increased number of GO bilayers (Figure 8b). XPS analysis revealed that there is no trace of chlorine detected for the GO_{10} multilayer assembled on a planar silicon surface after exposure to chlorine for 1 h. The chlorine content of the GO_{10}-coated PA membrane was estimated to be 2.3 ± 0.3, which is much less than that of the uncoated one (5.5 ± 1.4), indicating that the presence of the GO multilayer disfavors chlorine uptake. It should be noted that some amount of chlorine detected for the GO_{10}-coated PA membrane is attributed due to incomplete GO coverage on the PA surface. Although in-depth structural characterization of the GO layer (e.g., GO interlayer spacing, GO functionality) is further needed to elucidate the molecular transport mechanism in the GO coating in conjunction with chlorine attack, it is reasonable to postulate that the chemically robust GO coating on the membrane surface could shield chlorine attack to some degree and retard its subsequent diffusion toward the inner PA region through the top of the PA layer. The rejection mechanism of the GO multilayer was reported to involve size exclusion determined by the GO interlayer spacing and electrostatic interaction (charge effect).[20,22] In particular, size exclusion could play a dominant role in discriminating active chlorine species (OCl^- ion), compared to the salt ion (Cl^-), since both ions are monovalent: Diffusion of the larger OCl^- ion through the GO multilayer is expected to be more restricted than the smaller Cl^- ion. As a result, the GO multilayers possibly could serve as an effective barrier that slows the penetration of active chlorine species toward the underlying PA, although it exhibited a relative low rejection of NaCl salt. In our study, the retarded diffusion of active chlorine species by the GO coating appears to be effective enough to delay performance deterioration, particularly in the early stage of chlorination (for less than 1 h), where the chlorine penetration depth does not overreach the inner core layer within the PA selective layer. For the pristine PA membrane at this stage, the degradation by chlorine would be already propagated to the inner core region to some degree, resulting in a significant reduction in salt rejection. However, since continuous exposure to chlorine would degrade salt rejection by destroying the inner core region after the critical period of chlorination time, the protective role of the GO coating in retarding selectivity loss could become lessened with increasing chlorination time and ultimately no longer effective at the highest chlorine dose, as illustrated in Figure 8b. This result suggests that the GO coating is likely to restrict the chlorine diffusion, rather than completely block its passage.

The chlorine attack and its penetration into the PA structure presumably take place through both outmost sides of the PA layer during the typical soaking experiment for chlorination: top side (directly contacting with chlorine) and bottom side (contacting with chlorine that is diffused through the pore structure of the underlying porous support). Although the GO coating can retard the chlorine penetration through the top side of the PA selective layer, chlorine degradation could progress through its bottom side and further reduce the overall PA network density, leading to a considerable increase in water flux.

To confirm our hypothesis, we laid the GO multilayers underneath the PA selective layers of the pristine PA and GO_{10}-coated PA membranes by LbL deposition of AGO and GO nanosheets prior to interfacial polymerization to prepare GO_{10}-underlaid PA and GO_{10}-sandwiched PA membranes, respectively, and compared their performance changes upon chlorination (see Figure 9). Similar to the case of the GO_{10}-coated PA membrane, the GO_{10}-underlaid PA membrane showed the highly suppressed selectivity loss along with a slightly retarded flux increase, compared to those of the pristine one upon chlorination. In addition, the GO_{10}-sandwiched PA membrane led to further suppression in flux increase while maintaining the high retention level of salt rejection after chlorination, in comparison with those of one-side-coated (i.e., GO-coated or GO-underlaid) PA membranes. These experimental results strongly support our argument that the PA structural damage by chlorine attack occurs through both sides of the PA layer.

We further examined the role of the GO layer in chlorine-induced degradation under the more-realistic cleaning condition where membranes are exposed to the pressurized chlorine solution during the filtration (see Figure S3 in the Supporting Information). Although the rate of reduction in NaCl rejection was accelerated when membranes were exposed to the pressurized chlorine solution (chlorine concentration = 100 mg/L), in comparison with the case of soaking membranes

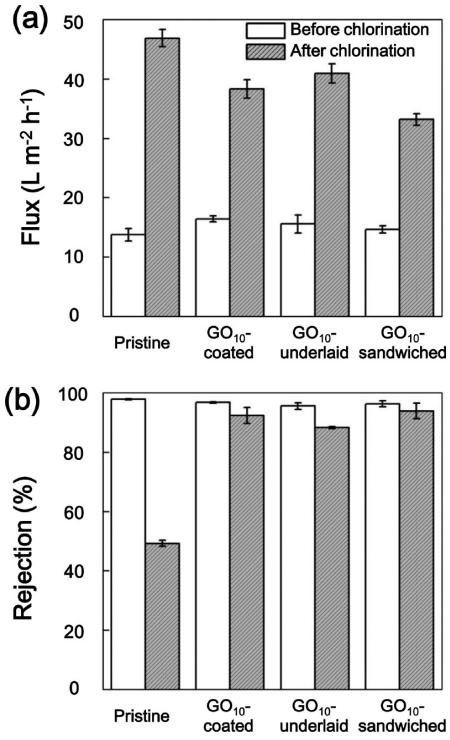

Figure 9. (a) Water flux and (b) NaCl rejection of the pristine, uncovered polyamide (PA), GO_{10}-coated PA, GO_{10}-underlaid PA, and GO_{10}-sandwiched PA membranes before and after chlorine exposure for 1 h (chlorination conditions: chlorine concentration = 6000 mg/L and pH 10).

into chlorine solution, the presence of the GO layer was found to remarkably retard the selectivity loss of the PA membranes, even for the pressurized chlorine exposure.

CONCLUSION

In summary, we have developed a dual-action durable coating strategy to improve resistance to both fouling and chlorine-induced degradation of polyamide−thin-film composite (PA-TFC) membranes via layer-by-layer (LbL) deposition of graphene oxide (GO) nanosheets. In contrast to conventional coatings that typically cause a flux decline, the membrane permeability was not altered by the LbL-assembled GO coating, presumably because of the unique water transport between GO nanosheets. The GO coating mitigated membrane fouling by rendering the membrane surface more hydrophilic and/or smoother. In addition, the chemically robust nature of GO enables the GO coating layer to act as a protective layer for the underlying PA structure upon chlorination, which maintained the high level of salt rejection. The improved chlorine stability of the GO-coated PA membrane was ascribed to the impeding role of GO coating layers through which diffusion of the reactive chlorine species was retarded before eventually reaching and disrupting the core region of PA layers. The unique functions offered by the GO multilayered coating could be utilized to develop a new class of highly durable and highly permeable membranes for desalination and water treatment.

ASSOCIATED CONTENT

Supporting Information

This material is available free of charge via the Internet at http://pubs.acs.org.

AUTHOR INFORMATION

Corresponding Authors

*E-mail: jungkyu_choi@korea.ac.kr (J.C.).
*E-mail: joona@korea.ac.kr (J.B.).
*E-mail: leejhy@kist.re.kr (J.-H.L.).

Notes

The authors declare no competing financial interest.

ACKNOWLEDGMENTS

This research was supported by the KIST Institutional Programs (Project Nos. 2E23900, 2V03280) and also by National Research Foundation of Korea grant funded by the Korea government (MSIP) (Nos. 2012R1A2A2A01014473 and 2012M3A7B4049863) and also by the Global Frontier R&D Program (No. 2013-073298) on Center for Hybrid Interface Materials (HIM) funded by the Ministry of Science, ICT & Future Planning. J.C. acknowledges the support by the Korea CCS R&D Center (KCRC) grant funded by the Korea government (Ministry of Science, ICT & Future Planning) (No. 2011-0032167).

REFERENCES

(1) Elimelech, M.; Phillip, W. A. *Science* **2011**, *333*, 712−717.
(2) Feinberg, B. J.; Ramon, G. Z.; Hoek, E. M. V. *Environ. Sci. Technol.* **2013**, *47*, 2982−2989.
(3) Geise, G. M.; Lee, H. S.; Miller, D. J.; Freeman, B. D.; Mcgrath, J. E.; Paul, D. R. *J. Polym. Sci., Part B: Polym. Phys.* **2010**, *48*, 1685−1718.
(4) Misdan, N.; Lau, W. J.; Ismail, A. F. *Desalination* **2012**, *287*, 228−237.
(5) Rana, D.; Matsuura, T. *Chem. Rev.* **2010**, *110*, 2448−2471.
(6) Zhao, L.; Chang, P. C. Y.; Yen, C.; Ho, W. S. W. *J. Membr. Sci.* **2013**, *425*, 1−10.
(7) Ishigami, T.; Amano, K.; Fujii, A.; Ohmukai, Y.; Kamio, E.; Maruyama, T.; Matsuyama, H. *Sep. Purif. Technol.* **2012**, *99*, 1−7.
(8) Kang, G. D.; Yu, H. J.; Liu, Z. N.; Cao, Y. M. *Desalination* **2011**, *275*, 252−259.
(9) Sagle, A. C.; Van Wagner, E. M.; Ju, H.; McCloskey, B. D.; Freeman, B. D.; Sharma, M. M. *J. Membr. Sci.* **2009**, *340*, 92−108.
(10) Wei, X. Y.; Wang, Z.; Zhang, Z.; Wang, J. X.; Wang, S. C. *J. Membr. Sci.* **2010**, *351*, 222−233.
(11) Lee, H. S.; Im, S. J.; Kim, J. H.; Kim, H. J.; Kim, J. P.; Min, B. R. *Desalination* **2008**, *219*, 48−56.
(12) Park, J.; Choi, W.; Kim, S. H.; Chun, B. H.; Bang, J.; Lee, K. B. *Desalin. Water Treat.* **2010**, *15*, 198−204.
(13) Colquhoun, H. M.; Chappell, D.; Lewis, A. L.; Lewis, D. F.; Finlan, G. T.; Williams, P. J. *J. Mater. Chem.* **2010**, *20*, 4629−4634.
(14) Nie, F. Q.; Xu, Z. K.; Ye, P.; Wu, J.; Seta, P. *Polymer* **2004**, *45*, 399−407.
(15) Park, H. B.; Freeman, B. D.; Zhang, Z. B.; Sankir, M.; McGrath, J. E. *Angew. Chem., Int. Ed.* **2008**, *47*, 6019−6024.
(16) Xu, J.; Wang, Z.; Yu, L. L.; Wang, J. X.; Wang, S. C. *J. Membr. Sci.* **2013**, *435*, 80−91.
(17) Glater, J.; Hong, S. K.; Elimelech, M. *Desalination* **1994**, *95*, 325−345.
(18) Dreyer, D. R.; Park, S.; Bielawski, C. W.; Ruoff, R. S. *Chem. Soc. Rev.* **2010**, *39*, 228−240.
(19) Cohen-Tanugi, D.; Grossman, J. C. *Nano Lett.* **2012**, *12*, 3602−3608.
(20) Hu, M.; Mi, B. X. *Environ. Sci. Technol.* **2013**, *47*, 3715−3723.
(21) Nair, R. R.; Wu, H. A.; Jayaram, P. N.; Grigorieva, I. V.; Geim, A. K. *Science* **2012**, *335*, 442−444.
(22) Han, Y.; Xu, Z.; Gao, C. *Adv. Funct. Mater.* **2013**, *23*, 3693−3700.
(23) Li, H.; Liang, S.; Li, J.; He, L. *J. Mater. Chem. A* **2013**, *1*, 6335−6341.

(24) Kim, H. W.; Yoon, H. W.; Yoon, S. M.; Yoo, B. M.; Ahn, B. K.; Cho, Y. H.; Shin, H. J.; Yang, H.; Paik, U.; Kwon, S.; Choi, J. Y.; Park, H. B. *Science* **2013**, *342*, 91−95.
(25) Li, H.; Song, Z. N.; Zhang, X. J.; Huang, Y.; Li, S. G.; Mao, Y. T.; Ploehn, H. J.; Bao, Y.; Yu, M. *Science* **2013**, *342*, 95−98.
(26) Dikin, D. A.; Stankovich, S.; Zimney, E. J.; Piner, R. D.; Dommett, G. H. B.; Evmenenko, G.; Nguyen, S. T.; Ruoff, R. S. *Nature* **2007**, *448*, 457−460.
(27) Cicero, G.; Grossman, J. C.; Schwegler, E.; Gygi, F.; Galli, G. *J. Am. Chem. Soc.* **2008**, *130*, 1871−1878.
(28) Jeong, H. K.; Lee, Y. P.; Lahaye, R. J. W. E.; Park, M. H.; An, K. H.; Kim, I. J.; Yang, C. W.; Park, C. Y.; Ruoff, R. S.; Lee, Y. H. *J. Am. Chem. Soc.* **2008**, *130*, 1362−1366.
(29) Huang, W. J.; Taylor, S.; Fu, K. F.; Lin, Y.; Zhang, D. H.; Hanks, T. W.; Rao, A. M.; Sun, Y. P. *Nano Lett.* **2002**, *2*, 311−314.
(30) Lee, D. W.; Hong, T. K.; Kang, D.; Lee, J.; Heo, M.; Kim, J. Y.; Kim, B. S.; Shin, H. S. *J. Mater. Chem.* **2011**, *21*, 3438−3442.
(31) Ramanathan, T.; Fisher, F. T.; Ruoff, R. S.; Brinson, L. C. *Chem. Mater.* **2005**, *17*, 1290−1295.
(32) Park, J.; Park, J.; Kim, S. H.; Cho, J.; Bang, J. *J. Mater. Chem.* **2010**, *20*, 2085−2091.
(33) Ang, W. S.; Lee, S. Y.; Elimelech, M. *J. Membr. Sci.* **2006**, *272*, 198−210.
(34) Marcano, D. C.; Kosynkin, D. V.; Berlin, J. M.; Sinitskii, A.; Sun, Z. Z.; Slesarev, A.; Alemany, L. B.; Lu, W.; Tour, J. M. *ACS Nano* **2010**, *4*, 4806−4814.
(35) Paredes, J. I.; Villar-Rodil, S.; Martinez-Alonso, A.; Tascon, J. M. D. *Langmuir* **2008**, *24*, 10560−10564.
(36) Si, Y.; Samulski, E. T. *Nano Lett.* **2008**, *8*, 1679−1682.
(37) Stankovich, S.; Piner, R. D.; Nguyen, S. T.; Ruoff, R. S. *Carbon* **2006**, *44*, 3342−3347.
(38) Kang, G. D.; Gao, C. J.; Chen, W. D.; Jie, X. M.; Cao, Y. M.; Yuan, Q. *J. Membr. Sci.* **2007**, *300*, 165−171.
(39) Zhou, Y.; Yu, S.; Gao, C. J.; Feng, X. S. *Sep. Purif. Technol.* **2009**, *66*, 287−294.
(40) Bagri, A.; Mattevi, C.; Acik, M.; Chabal, Y. J.; Chhowalla, M.; Shenoy, V. B. *Nat. Chem.* **2010**, *2*, 581−587.
(41) Ghosh, A. K.; Jeong, B. H.; Huang, X. F.; Hoek, E. M. V. *J. Membr. Sci.* **2008**, *311*, 34−45.
(42) Vrijenhoek, E. M.; Hong, S.; Elimelech, M. *J. Membr. Sci.* **2001**, *188*, 115−128.
(43) Muller, M.; Rieser, T.; Lunkwitz, K.; Meier-Haack, J. *Macromol. Rapid Commun.* **1999**, *20*, 607−611.
(44) Do, V. T.; Tang, C. Y. Y.; Reinhard, M.; Leckie, J. O. *Environ. Sci. Technol.* **2012**, *46*, 852−859.
(45) Lee, J. H.; Chung, J. Y.; Chan, E. P.; Stafford, C. M. *J. Membr. Sci.* **2013**, *433*, 72−79.
(46) Cahill, D. G.; Freger, V.; Kwak, S. Y. *MRS Bull.* **2008**, *33*, 27−32.
(47) Coronell, O.; Marinas, B. J.; Cahill, D. G. *Environ. Sci. Technol.* **2011**, *45*, 4513−4520.
(48) Freger, V. *Langmuir* **2003**, *19*, 4791−4797.
(49) Freger, V. *Environ. Sci. Technol.* **2004**, *38*, 3168−3175.